# Nanoparticles in Neuro-Oncology Theranostics

The rapid growth of nanotechnology and the development of novel nanomaterials with unique physicochemical characteristics provides potential for the utility of nanomaterials in theranostics, including neuroimaging, for identifying neurodegenerative changes or central nervous system malignancy.

## 1. Introduction

The rapid growth of nanotechnology and the development of novel nanomaterials with unique physicochemical characteristics provides potential for the utility of nanomaterials in theranostics, including neuroimaging, for identifying neurodegenerative changes or central nervous system malignancy. Theranostic agents play an important and emerging role in the diagnostics and treatment of metastatic tumors, allowing for refinement and reduction of treatment intervention of the cancer patient, and the combination of theranostic agents with nanoparticles has been an area of active research in the past few years. The small size and large surface area of nanomaterials permits translocation across biological barriers and enhances the interaction with cellular and intracellular components of tumor cells and the tumor microenvironment. In any other context, such extravasation would be considered undesirable, especially when not targeted, but in the context of cancer theranostics this is a tremendously useful property. The current lack of literature investigating the modifications necessary to properly target these nanoparticles, especially to the neuro-oncology space, as well as the lack of literature on nanoparticles' imaging visibility and interactions and the off-target toxic potential of such nanomaterials limits their effective clinical translation. For the CNS oncology scope, the brain poses several challenges for treatment, including the limitations on toxicity that could lead to neurodegeneration of native cells, thereby impacting patient mortality and morbidity greatly.

Theranostic agents for the CNS follow the same criteria to achieve clinically relevant levels in the brain or in a primary/metastatic tumor site. **Figure 1** illustrates the general scope of nanoparticles that have been developed, each focused on specific characteristics that optimally allow for specific drug delivery. The use of nanoparticles allows for both the targeting of nanoparticles for use in imaging of tumor location and size, as well as delivery of a therapeutic agent, which could be a small chemotherapeutic agent or a radioactive isotope (**Figure 1**B,C). The traditional formulation system for nanoparticles in theranostic delivery is the packaging of a compound into a nanoparticle, alone or in conjunction with a targeting ligand, e.g., gadolinium and an antibody for targeting to a specific receptor (**Figure 1**D).
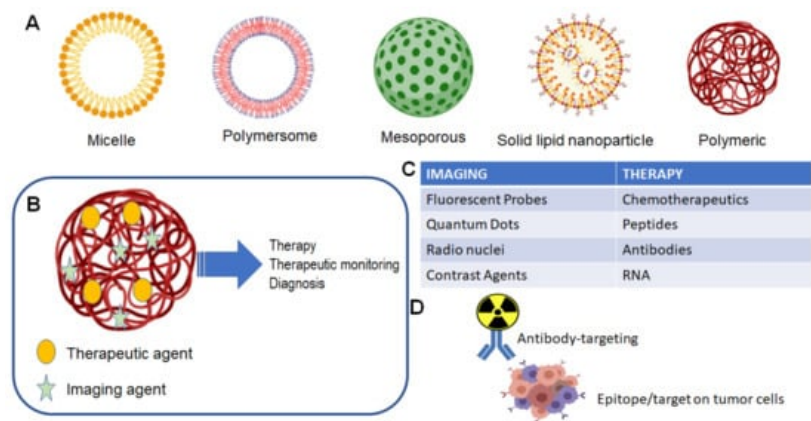


**Figure 1.** Nanoparticle and theranostic delivery. (**A**) Several nanoparticle systems have been described, each suited for optimal delivery and targeting of therapeutic agents [1][2]. (**B**) The theranostic nanoparticle can be formulated to include both an imaging agent and therapeutic agent [1]; (**C**) several options are available for either imaging of tumor and treatment of tumor [1]; (**D**) classical theranostic agent with radioactive cargo delivered to tumor via antibody targeting [3].

## 2. Use of Nanoparticles as a Diagnostic Imaging Tool

This section describes the results of our literature search for studies regarding the use of nanoparticles as contrast agents with which a variety of medical imaging modalities can view a variety of tumor types. This should be prefaced with the understanding that nearly all of these studies were conducted to view tumors xenografted into a murine (mouse) model. Additionally, the vast majority of our results were descriptions of successful use, rather than head-to-head comparisons of nanoparticles. Those that did list comparative data were those looking at the effect of an addition to or modification of a base nanoparticle (i.e., A vs. A + B). Thus, it was not reasonable to draw conclusions about the utility of one nanoparticle vs. another.

### 2.1. MRI

Our review of the literature shows that magnetic resonance imaging (MRI) as an imaging modality has seen the largest variety of nanoparticles used as either carriers for agents that provide contrast or as direct contrast agents themselves. Single wall carbon nanotubes (SWCNT) are the first example of the former. These agents have been transfected with molecules known to provide contrast on MRI, such as manganese [4], gadolinium [5][6][7], and iron oxide [8][9][10], in order to visualize tumor types including 4T1 breast carcinoma [4][8][9][10] and S180 sarcoma [5][6][7]. In a similar molecular sense, multiwalled carbon nanotubes (MWCNT) have also been successfully utilized as carriers for iron oxide [11][12][13][14][15] and gadolinium [16]. These agents have aided in the visualization of xenografts consisting of KB cell tumors, human breast carcinomas (MCF-7 cell line), and hepatocellular carcinomas. Another carbon-based agent, the magnetic hollow porous carbon nanoparticle (MHPCN), is an interesting compound of carbon nanodots and iron oxide that has been studied as an MRI contrast agent for visualizing human cervical carcinoma [17]. Iron oxide has also been paired with graphene oxide nanosheets and has been successfully used to produce contrast in 4T1 breast carcinoma [18][19]. Whether these carbon-based particles and their paired metals act in synergism to enhance contrast is an interesting question. A study by Fu et al. demonstrated enhanced contrast on MRI when graphene oxide was transfected with iron oxide and compared with the contrast produced by graphene oxide alone [20]. Furthermore, Rammohan et al. showed that when gadolinium was paired with nanodiamonds, relaxivity was increased 10-fold compared with that of gadolinium alone [21].

Looking at agents that stray further from a carbon-based carrier, some of the aforementioned attached particles were popular in our search. Iron oxide has been used alone as an MRI contrast agent for imaging models of nasopharyngeal and breast carcinoma [22]. More frequently, iron oxide has served to provide MRI contrast while combined with other particles of varying utility. Examples include combination with iron-platinum nanoparticles in visualizing epidermoid and breast carcinoma [23], doping with zinc particles to improve contrast in breast carcinoma [24], formation of zinc–cobalt–ferrite nanoparticles to enhance the contrast effect seen with iron oxide alone in melanoma (C540 cell line) [25], and pairing with upconversion nanoparticles and gold particles in a dual modal imaging and photothermal therapy agent for breast carcinoma [26]. Perhaps the most common utilization of iron oxide as an MRI contrast agent has been as part of larger multi-agent nanoparticles with multimodal imaging and even therapeutic capability. To spare redundancy, the individual utility of the contrast agents in each example are listed in their respective imaging utility subsections later in this work, described as part of multimodal imaging nanoparticles also. Important to recognize are the many different particles iron oxide has been compounded with while still maintaining its ability to successfully provide contrast in tumors visualized with MRI. Iron oxide has filled this role in a number of combinations to include: silver sulfide and a near-infrared (NIR) fluorophore to visualize breast carcinoma [27]; tantalum oxide, copper sulfide, and zinc phthalocyanine to image cervical carcinoma (U14 cell line) [28]; fluorescent semiconducting polymer to image cervical carcinoma (HeLa cell line) [29]; dimercaptosuccinic acid, bevacizumab, and technetium-99m to view breast carcinoma [30]; bovine lactoferrin and VivoTag 680 to visualize colon carcinoma (Caco-2 cell line) [31]; upconversion nanoparticles (Y, Yb, Er) and squaraine dye to view 4T1 breast carcinoma [32]; polydopamine particles and DNA probes to image breast carcinoma (MCF-7 cell line) [33]; molybdenum disulfide nanosheets to view breast carcinoma [34]; and polypyrrole to again view breast carcinoma [35].

Gadolinium as we know is commonly used in medical imaging as an MRI contrast agent. It has thus been employed for this use in a number of nanoparticle compounds other than the carbon-based carriers. In a study using titanium dioxide for sonodynamic therapy of prostate adenocarcinoma (LNCaP cell line), gadolinium was attached specifically to provide MRI utility [36]. It served the same purpose when attached to a zinc oxide quantum dot template that was being used for fluorescent imaging of a pancreatic carcinoma (BxPC-3 cell line) [37]. Using a keratin template, gadolinium has been combined with manganese dioxide to achieve an enhanced T1-weighted MRI effect in 4T1 breast carcinoma due to optimal structure on the template and the combination effect of two MRI contrast agents [38]. Zhong et al. created a scintillating nanoparticle composed of $NaCeF_4$:GdTb and proposed that the presence of lanthanide Ce and Tb ions actually enhanced the MRI contrast capability of gadolinium in lung carcinoma (A549 cell line) [39]. Similarly, Wang et al.

added gadolinium to expand the multimodal imaging capabilities of their upconversion nanoparticle $NaYF_4/NaGdF_4$ to enhance MRI visualization of cervical carcinoma (HeLa cell line) [40].

Manganese is an element that displays utility as an MRI contrast agent, often as the $Mn^{2+}$ ion or as manganese dioxide. It has actually been reported that manganese dioxide will react with increased $H^+$ and GSH found in the tumor microenvironment to yield $Mn^{2+}$, increasing the observed T1-weighted relaxivity [38][41]. As such, a list of studies exists in which either is utilized to add MRI functionality to the designed nanoparticle. $Mn^{2+}$ has been added to a calcium carbonate carrier along with chlorin e6 and a polydopamine coat to view 4T1 breast carcinoma [42]; added to a polydopamine carrier along with indocyanine green and doxorubicin for theranostic study of 4T1 breast carcinoma [43]; combined with polydopamine coated black titanium dioxide and chlorin e6 for theranostic study of 4T1 breast carcinoma [44]; combined with gold, titanium dioxide, and doxorubicin for theranostic study of cervical carcinoma (HeLa cell line) [45]; fabricated with a near-infrared dye to form a nanoscale metal-organic particle and coated with polydopamine for theranostic study of breast carcinoma [46]; combined with collagenase with the goal of degrading the tumor ECM for better perfusion and imaging of breast carcinoma [47]; and combined with calcium carbonate and doxorubicin for theranostic study of breast carcinoma [48]. Manganese dioxide has been combined with chlorin e6 and doxorubicin for theranostic study of 4T1 breast carcinoma [41]; and attached to keratin carrier surface along with gadolinium oxide and doxorubicin for theranostic study of 4T1 breast carcinoma [38]. Two unique applications of manganese were also uncovered in our search. One of which used manganese in combination with tungsten to create a bimetallic oxide (MnWOx) for the purpose of sonodynamic therapy enhancement as well as imaging of 4T1 breast carcinoma [49]. The other used manganese sulfide (MnS) and combined it with zinc sulfide and gold for theranostic study of breast carcinoma [50].

Finally, there are two miscellaneous molecules that, while less popular, have been incorporated into nanoparticles for purposes of providing contrast on magnetic resonance imaging. Titanium dioxide has been combined with Yb, Ho, and F to form an upconversion nanoparticle useful for imaging breast carcinoma (MCF-7 cell line) [51], and vanadium disulfide nanodots have been paired with technetium-99 for theranostic study of 4T1 breast carcinoma [52].

Briefly, we verify that various nanoparticles have been successfully used to produce contrast in brain tumor models as well. One review describing the imaging of various glioma/glioblastoma models reported the use of several agents to produce contrast on MRI, including gadolinium, iron oxide, and gold nanoparticles [53]. In another review, various brain tumors are reported to have been imaged using iron oxide, gadolinium, and manganese oxide nanoparticles [54].

## 2.2. CT

Computed tomography (CT) as an imaging modality did not yield as many results in our search as those for MRI, perhaps because of the sharp image quality MRI provides, particularly for soft tissues (i.e., tumors). Nonetheless, a number of studies were found using a variety of miscellaneous nanoparticles as contrast agents under CT imaging of tumors. Some of these were used specifically for CT imaging, but many were constructed for multimodal imaging or theranostic use. Several of the lanthanide elements have been incorporated into two examples of nanoparticles used for CT imaging. The same scintillating nanoparticle composed of Ce, Gd, and Tb ions found useful for MRI also provided contrast for CT imaging of lung carcinoma (A549 cell line) [39]. Similarly, the aforementioned Gd containing upconversion nanoparticle $NaYF_4/NaGdF_4$ used for MRI also provided CT contrast for cervical cancer (HeLa cell line) [40]. Titanium compounds have been rendered useful for CT contrast as well. Growing gold on the surface of titanium carbide allowed CT imaging of 4T1 breast carcinoma [55], and doping titanium dioxide with tungsten allowed CT imaging of the same [56]. The MnWOx nanoparticle that had MRI capability also saw utility as a CT contrast agent from the presence of tungsten [49]. Iron oxide was useful in two multimodal imaging studies that included CT imaging. One combined iron oxide with bovine lactoferrin, alginate-enclosed chitosan-encapsulated calcium phosphate, and Vivotag 680 for theranostic study of colon cancer (Caco-2 cell line) [31]. The other included an NIR-fluorophore and silver sulfide that served to enhance the CT contrast effect of iron oxide in breast carcinoma [27]. Tantalum oxide doped with iron, presumably with combined effect, provided CT contrast ability to the multimodal nanoparticle also consisting of copper sulfide and zinc phthalocyanine for theranostic study of cervical carcinoma (U13 cell line) [28]. Rhenium sulfide was used as a lone agent to view 4T1 breast carcinoma [57]. A bismuth–carbon nanoparticle composite was constructed as a naïve compound for imaging cervical carcinoma (HeLa cell line) [58]. Nanoscale coordination polymers of hafnium and bis-alkene as CT contrast agents were compounded with doxorubicin and chlorin e6 for theranostic study of breast carcinoma [59]. Finally, our search yielded a study using ExiTron nano, an alkaline earth-based nanoparticulate contrast agent manufactured by Viscover, to view liver metastases of an unspecified tumor of origin [60]. In terms of brain-tumor-specific imaging, gold nanoparticles have been successfully used as CT contrast agents in a U87 malignant glioma model [53].

## 2.3. Fluorescent and NIR Fluorescent Imaging

Here we describe findings for fluorescent and NIR fluorescent imaging, the difference being the use of light in the near-infrared (NIR) spectrum vs. shorter wavelengths. NIR fluorescence carries the advantages of deeper tissue penetration and less autofluorescence from surrounding tissues (low background), making it the intuitively preferred modality for tumor imaging [61]. Nonetheless, our search yielded studies describing the use of each.

Zinc oxide has been useful as a fluorescent imaging agent in two forms from our search. Zinc oxide quantum dots added fluorescent imaging utility to the multimodal nanoparticle used for theranostic study of pancreatic cancer (BxPC-3 cell line) [37], and a hollow zinc oxide nanocarrier of paclitaxel and folate allowed fluorescent imaging in a theranostic study of breast carcinoma [62]. Iron oxide nanoparticles are not used directly as agents for fluorescent imaging but rather can serve as the core particle and thus the carrier for agents that provide fluorescence. In one multimodal imaging study, iron oxide was encapsulated with a semiconducting polymer that provided fluorescent capability for viewing cervical cancer (HeLa cell line) [29]. A multimodal combination of iron oxide and an upconversion nanoparticle served as a carrier for squaraine dye, an agent used for downconversion fluorescent imaging of 4T1 breast carcinoma [32]. Taking advantage of the fluorescent capacity of zinc, an iron oxide–polydopamine nanoparticle was transfected with a DNA probe tasked with increasing intracellular release of endogenous zinc for imaging of breast carcinoma (MCF-7 cell line) [33]. Manganese dioxide has served a similar role in a multimodal theranostic study using a hollow manganese dioxide nanoplatform as a carrier for doxorubicin and chlorin e6 as the fluorescent agent to view 4T1 breast carcinoma [41]. The multimodal MnWOx nanoparticle used for theranostic study of 4T1 breast carcinoma was also turned into a fluorescent agent due to the attachment of DiR iodide dye [49]. Graphene oxide has served as carrier for attachments of iron oxide and the fluorescent agent cyanine 5 for viewing 4T1 breast carcinoma [19]. Titanium dioxide doped with Yb, Ho, and F showed utility for upconversion fluorescent imaging of breast carcinoma (MCF-7 cell line) [51]. A titanium dioxide polypyrrole nanoparticle conjugated with DiR fluorescent dye was used to successfully image ovarian carcinoma (Skov3 cell line) [63]. The previously discussed scintillating nanoparticle composed of $NaCeF_4$:GdTb was endowed with X-ray excited fluorescence for imaging of lung carcinoma (A549 cell line) due to the presence of terbium ions [39]. SWCNT when used for fluorescent imaging have been conjugated with a fluorophore such as chlorin e6 when viewing squamous cell carcinoma [64] or a cyanine 5-labeled aptamer to view xenograft tumors of ALL or Burkitt's lymphoma [65]. Finally, small molecule gold nanoparticles found use in a study viewing lung carcinoma [66].

SWCNT have been studied extensively as NIR fluorescent imaging contrast agents, occasionally with a fluorescent dye attached or a structural change. This is due to their good optical absorbance in the NIR region [67], though only a subset of nanotube chiralities will actually fluoresce or heat well under a NIR laser on their own [68]. A few examples of naïve SWCNT, or those without dye or structural alterations, include isolates of these chiralities. These are typically used in the NIR-II region. Diao et al. viewed the vasculature of 4T1 breast carcinoma by specifically isolating the (12, 1) and (13, 3) chiralities of SWCNT which demonstrate ~5-fold higher photoluminescence than unsorted SWCNT [69]. Antaris et al. isolated the (6, 5) chirality of SWCNT to view 4T1 breast carcinoma, and this isolate displayed 6-fold brighter luminescence than unsorted SWCNT [68]. Two studies chose to stabilize unsorted SWCNT for NIR-II imaging with an M13 bacteriophage, and found that this allowed the unsorted nanotubes to provide good fluorescence for viewing prostate adenocarcinoma [70] and ovarian carcinoma (OVCAR8 cell line) with tumor-to-background ratio actually 24- and 28-fold higher than standard NIR fluorescent dyes AF750 and FITC [71]. Another study took advantage of both a nanofluorophore and SWCNT without actually combining them. In this work, unsorted SWCNT were used to image a 4T1 breast carcinoma tumor via the enhanced permeability and retention effect, and a nanofluorophore called p-FE was created to visualize the tumor vasculature. These agents emitted two different colors of fluorescence, and the unsorted SWCNT had to be given at a high dose with 5-fold longer imaging exposure time and 2-fold larger pinhole on the imaging device to capture fluorescence emission [72]. The intrinsic NIR properties of unsorted SWCNT were used alone with no fluorescent dye in the imaging of breast carcinoma [73]. Functionalization via structural change to both SWCNT and graphene nanosheets with the addition of poloxamer 407 has been used to image squamous cell carcinoma by NIR fluorescence [74]. A semiconducting SWCNT with large diameter has been used to view breast carcinoma as well as cerebrovascular flow [75]. Several studies have employed the attachment of a fluorescent dye to enhance NIR fluorescent capability of SWCNT. These include the addition of Alexa Fluor 594 to view ovarian carcinoma [76], cyanine 7 to view pancreatic carcinoma (BxPC-3 cell line) [67], cyanine 5.5 to view breast carcinoma (MCF-7 cell line) [77], IR-783 to view sarcoma (S180 cell line) [6], and DiR to view sarcoma (S180 cell line) [7].

Several other agents have been employed for NIR fluorescence study as well, many being fluorescent dyes expanding the imaging capability of other nanoparticles. Graphene oxide with an attachment of cyanine 5.5 has been used for imaging 4T1 breast carcinoma [78]. Multimodal iron oxide has been rendered useful for NIR fluorescent imaging via attachment of the fluorescent dye VivoTag 680 to image colon carcinoma (Caco-2 cell line) [31]. The NIR fluorophore DiR has been incorporated into a PEGylated phospholipid mixed micel also containing iron oxide and silver sulfide in order to expand imaging capabilities of breast carcinoma [27]. The NIR fluorescent dye IR825 has been attached to manganese

nanoscale metal–organic particles [46] and to human serum albumin [79] for imaging of breast carcinoma in both cases. Chlorin e6 was attached to a multimodal calcium carbonate carrier for imaging of 4T1 breast carcinoma [42]. Titanium dioxide was rendered capable of NIR fluorescent imaging of tumors, interestingly by doping with $Nb^{5+}$ ions, which caused the molecule's light absorption capacity to shift into the NIR region [80]. One study actually simplified the approach, citing problems of low brightness and low fluorescence quantum yield of previous carrier-based systems, with the NIR fluorescent dye NPAPF, which was prepared for administration alone with no carrier or attachments to image breast carcinoma [81]. Another study used a lone downconversion nanoparticle (NaYYbErF), attachments being molecules for tumor targeting and biostability, to view ovarian carcinoma (COV362 cell line) [82]. Finally, one study employed the use of fluorescent CdTe quantum dots in order to image KB tumor [83].

Various agents have been used specifically for fluorescent imaging of brain tumors as well. Glioma/glioblastoma models have been imaged using quantum dots [53][84], SWCNT [85], liposomal nanoparticles, and holotransferrin nanoparticles [53]. Polyacrylamide, iron oxide with Cy5.5 dye, and quantum dots again were reported as agents used to image various tumors and tumor vasculature. It should be noted, however, that the skull proves to be a significant physical barrier to fluorescent imaging, and the utility of this modality is mainly isolated to intraoperative localization of brain tumor tissue [54].

## 2.4. Photoacoustic Imaging

SWCNT are popular contrast agents for photoacoustic (PA) imaging as well, again secondary to their responsiveness to light in the NIR region [64][86]. Although some studies attached agents to SWCNT in order to enhance PA imaging, SWCNT were the sole mode of contrast in a study imaging squamous cell carcinoma [64]. One study took the approach of attaching PA contrast dyes to SWCNT, creating five separate "flavors" of nanoparticles, those including $QSY_{21}$ and indocyanine green exhibiting over 100-fold higher PA contrast than SWCNT alone [87]. Another study shared the mechanism of indocyanine green attachment for the imaging of 4T1 breast carcinoma, notably showing 2-fold greater enhancement with the SWCNT–indocyanine green combination than indocyanine green alone [88]. Other carbon-based nanoparticles useful for PA imaging include graphene oxide nanosheets, which served as PA contrast in two multimodal studies imaging 4T1 breast carcinoma [19][89], and hollow mesoporous carbon nanospheres, which did the same for two other theranostic xenograft studies [90][91]. Aside from carbon-based nanoparticles, our search yielded a mix of other agents that have been studied as PA contrast. Titanium dioxide has been modified several times to shift its absorption into the NIR range and to thus become useful for PA imaging. One example is from a previously mentioned study that utilized doping of titanium dioxide with tungsten in order to visualize 4T1 breast carcinoma [56]. Making titanium dioxide an oxygen-deficient molecule ($TiO_2$-x) also increased absorption in the NIR range, allowing PA imaging [92]. The same study that doped titanium dioxide with $Nb^{5+}$ ions for NIR fluorescent imaging found this to be useful for creating a PA contrast agent as well [80]. Gold nanorods display good absorption in the NIR range and thus have been used as PA contrast to image cervical carcinoma (HeLa cell line) [93]. Seeding of gold actually allowed functionalization of a titanium carbide nanosheet carrier for the imaging of 4T1 breast carcinoma [55]. The previously mentioned multimodal imaging study with calcium carbonate also reported good PA imaging of 4T1 breast carcinoma due to calcium carbonate having a polydopamine coat that expanded its utility [42]. $MoS_2$–iron oxide, a nanocomposite that showed utility as an MRI contrast agent, was also found to be useful for PA imaging of breast carcinoma [34]. In a theranostic study of cervical carcinoma (U14 cell line), a bismuth sulfide–manganese oxide nanocomposite served as the contrast agent [94]. The MRI contrast vanadium disulfide nanodots discussed earlier also show strong NIR absorbance and provide PA contrast of 4T1 breast carcinoma as well [52]. Finally, an interesting coordination polymer nanodot composed of ruthenium ions and phenanthroline, neither of which show significant optical absorbance alone, showed strong NIR absorbance as a compound allowing PA imaging of 4T1 breast carcinoma [95].

For brain tumor imaging, holotransferrin nanoparticles have served as PA contrast agents to view glioma models [53], and gold nanoparticles have been useful for viewing a variety of brain tumors [54]. Several studies have also utilized SWCNT for PA imaging of glioma/glioblastoma models [86][96][97]. Because of their close mechanistic relationship, PA and fluorescent imaging share the limitation imposed by the physical barrier of the skull.

## 2.5. PET Imaging

Due to the nature of the imaging mechanism, studies that included PET imaging of tumors attached a radiolabel to the nanoparticle under investigation. All but one chose the radioisotope [64] Cu. The study that differed used both 1,4,7,10-tetraazacyclododecane-1,4,7,10-tetraacetic acid (DOTA) and desferrioxamine B (DFO) as radiolabels attached to SWCNT for imaging colon adenocarcinoma (LS174T cell line) [98]. All of the following nanoparticles were transfected with [64] Cu for PET imaging: graphene oxide nanosheets in two studies viewing breast carcinoma [89][99], zinc oxide to image breast carcinoma [100], boron nitride nanoparticles in a therapeutic study of breast carcinoma [101], and molybdenum disulfide–iron oxide nanocomposite as previously mentioned to view breast carcinoma [34]. Iron oxide radiolabeled with [64] Cu has

been shown to provide contrast on PET for imaging various brain tumors [54], while SWCNT have been used to view a glioblastoma model [96].

### 2.6. SPECT Imaging

As with PET imaging, the use of the SPECT modality necessitates the addition of a radioisotope to the nanoparticle under study. Technetium-99 was the isotope of choice in most studies including the use of iron oxide [30], vanadium disulfide [52], and gallic acid–ferric nanocomplexes [102] to view breast carcinoma. Ref. [103] Iodine was the radioisotope attached in a multimodal imaging study using SWCNT to view breast carcinoma [4].

### 2.7. Miscellaneous

The remaining studies our search yielded cover a range of imaging modalities that were not as popular in the literature as those already mentioned. Only one study utilized X-ray imaging and did so by using gold as an X-ray absorber attached to graphene oxide for imaging breast carcinoma [18]. Two studies looked at ultrasound imaging, one of which used MWCNT as a contrast agent to visualize prostate carcinoma (CP-3 cell line) [104]. The other utilized pulsed magneto-motive ultrasound with zinc-doped iron oxide to provide magnetization and contrast for an epidermoid carcinoma (A431 cell line) [105]. A multimodal study utilized MWCNT as a contrast agent for MRI as well as microwave-induced thermoacoustic imaging of breast carcinoma [15]. Ref. [103] Iodine was attached to reduced graphene oxide nanoparticles for gamma imaging and IR thermal imaging of breast carcinoma [106]. Other nanoparticles used for IR thermal imaging include SWCNT [4] and iron oxide-polypyrrole [35], which both allowed visualization of breast carcinoma. A multimodal nanoparticle consisting of iron oxide, silver sulfide, and a NIR fluorophore successfully provided contrast for mammography due to the presence of silver sulfide [27]. Finally, magnetic particle imaging (MPI) was a modality explored with multimodal janus iron oxide ($Fe_3O_4$) to image cervical carcinoma. It was stated that the crystallinity of janus iron oxide allowed it to provide increased contrast on MPI compared with plain iron oxide ($Fe_2O_3$) [29].

## References

1. Madamsetty, V.S.; Mukherjee, A.; Mukherjee, S. Recent Trends of the Bio-Inspired Nanoparticles in Cancer Theranostics. Front. Pharmacol. 2019, 10, 1264.

2. Chen, F.; Ehlerding, E.B.; Cai, W. Theranostic nanoparticles. J. Nucl. Med. 2014, 55, 1919–1922.

3. Griffith, J.I.; Sarkaria, J.N.; Elmquist, W.F. Efflux Limits Tumor Drug Delivery Despite Disrupted BBB. Trends Pharmacol. Sci. 2021, 42, 426–428.

4. Zhao, H.; Chao, Y.; Liu, J.; Huang, J.; Pan, J.; Guo, W.; Wu, J.; Sheng, M.; Yang, K.; Wang, J.; et al. Polydopamine Coated Single-Walled Carbon Nanotubes as a Versatile Platform with Radionuclide Labeling for Multimodal Tumor Imaging and Therapy. Theranostics 2016, 6, 1833–1843.

5. Yan, C.; Chen, C.; Hou, L.; Zhang, H.; Che, Y.; Qi, Y.; Zhang, X.; Cheng, J.; Zhang, Z. Single-walled carbon nanotube-loaded doxorubicin and Gd-DTPA for targeted drug delivery and magnetic resonance imaging. J. Drug Target. 2016, 25, 163–171.

6. Zhang, Z.; Hou, L.; Yang, X.; Ren, J.; Wang, Y.; Zhang, H.; Feng, Q.; Shi, Y.; Shan, X.; Yuan, Y. A novel redox-sensitive system based on single-walled carbon nanotubes for chemo-photothermal therapy and magnetic resonance imaging. Int. J. Nanomed. 2016, 11, 607–624.

7. Zhang, Z.; Hou, L.; Wang, Y.; Yang, X.; Wang, L.; Zhang, H. Hyaluronic acid-functionalized single-walled carbon nanotubes as tumor-targeting MRI contrast agent. Int. J. Nanomed. 2015, 10, 4507–4520.

8. Al Faraj, A.; Shaik, A.S.; Al Sayed, B. Preferential magnetic targeting of carbon nanotubes to cancer sites: Noninvasive tracking using MRI in a murine breast cancer model. Int. J. Nanomed. 2015, 10, 931–948.

9. Al Faraj, A.; Shaik, A.P.; Shaik, A.S. Magnetic single-walled carbon nanotubes as efficient drug delivery nanocarriers in breast cancer murine model: Noninvasive monitoring using diffusion-weighted magnetic resonance imaging as sensitive imaging biomarker. Int. J. Nanomed. 2014, 10, 157–168.

10. Al Faraj, A.; Shaik, A.S.; Halwani, R.; Alfuraih, A. Magnetic Targeting and Delivery of Drug-Loaded SWCNTs Theranostic Nanoprobes to Lung Metastasis in Breast Cancer Animal Model: Noninvasive Monitoring Using Magnetic Resonance Imaging. Mol. Imaging Biol. 2015, 18, 315–324.

11. Lamanna, G.; Garofalo, A.; Popa, G.; Wilhelm, C.; Bégin-Colin, S.; Felder-Flesch, D.; Bianco, A.; Gazeau, F.; Ménard-Moyon, C. Endowing carbon nanotubes with superparamagnetic properties: Applications for cell labeling, MRI cell tracking and magnetic manipulations. Nanoscale 2013, 5, 4412.

12. Wang, L.; Shi, J.; Hao, Y.; Zhang, P.; Zhao, Y.; Meng, D.; Li, D.; Chang, J.; Zhang, Z. Magnetic Multi-Walled Carbon Nanotubes for Tumor Theranostics. J. Biomed. Nanotechnol. 2015, 11, 1653–1661.

13. Liu, Y.; Hughes, T.C.; Muir, B.; Waddington, L.J.; Gengenbach, T.R.; Easton, C.D.; Hinton, T.M.; Moffat, B.A.; Hao, X.; Qiu, J. Water-dispersible magnetic carbon nanotubes as T2-weighted MRI contrast agents. Biomaterials 2014, 35, 378–386.

14. Liu, Y.; Muir, B.; Waddington, L.J.; Hinton, T.M.; Moffat, B.A.; Hao, X.; Qiu, J.; Hughes, T.C. Colloidally Stabilized Magnetic Carbon Nanotubes Providing MRI Contrast in Mouse Liver Tumors. Biomacromolecules 2015, 16, 790–797.

15. Ding, W.; Lou, C.; Qiu, J.; Zhao, Z.; Zhou, Q.; Liang, M.; Ji, Z.; Yang, S.; Xing, D. Targeted Fe-filled carbon nanotube as a multifunctional contrast agent for thermoacoustic and magnetic resonance imaging of tumor in living mice. Nanomed. Nanotechnol. Biol. Med. 2016, 12, 235–244.

16. Wen, S.; Zhao, Q.; An, X.; Zhu, J.; Hou, W.; Li, K.; Huang, Y.; Shen, M.; Zhu, W.; Shi, X. Multifunctional PEGylated Multiwalled Carbon Nanotubes for Enhanced Blood Pool and Tumor MR Imaging. Adv. Healthcare Mater. 2014, 3, 1568–1577.

17. Wu, F.; Zhang, M.; Lu, H.; Liang, D.; Huang, Y.; Xia, Y.; Hu, Y.; Hu, S.; Wang, J.; Yi, X.; et al. Triple Stimuli-Responsive Magnetic Hollow Porous Carbon-Based Nanodrug Delivery System for Magnetic Resonance Imaging-Guided Synergistic Photothermal/Chemotherapy of Cancer. ACS Appl. Mater. Interfaces 2018, 10, 21939–21949.

18. Shi, X.; Gong, H.; Li, Y.; Wang, C.; Cheng, L.; Liu, Z. Graphene-based magnetic plasmonic nanocomposite for dual bioimaging and photothermal therapy. Biomaterials 2013, 34, 4786–4793.

19. Yang, K.; Hu, L.; Ma, X.; Ye, S.; Cheng, L.; Shi, X.; Li, C.; Li, Y.; Liu, Z. Multimodal Imaging Guided Photothermal Therapy using Functionalized Graphene Nanosheets Anchored with Magnetic Nanoparticles. Adv. Mater. 2012, 24, 1868–1872.

20. Fu, G.; Zhu, L.; Yang, K.; Zhuang, R.; Xie, J.; Zhang, F. Diffusion-Weighted Magnetic Resonance Imaging for Therapy Response Monitoring and Early Treatment Prediction of Photothermal Therapy. ACS Appl. Mater. Interfaces 2016, 8, 5137–5147.

21. Rammohan, N.; MacRenaris, K.W.; Moore, L.K.; Parigi, G.; Mastarone, D.J.; Manus, L.M.; Lilley, L.M.; Preslar, A.T.; Waters, E.A.; Filicko, A.; et al. Nanodiamond–Gadolinium(III) Aggregates for Tracking Cancer Growth In Vivo at High Field. Nano Lett. 2016, 16, 7551–7564.

22. Nan, X.; Zhang, X.; Liu, Y.; Zhou, M.; Chen, X.; Zhang, X. Dual-Targeted Multifunctional Nanoparticles for Magnetic Resonance Imaging Guided Cancer Diagnosis and Therapy. ACS Appl. Mater. Interfaces 2017, 9, 9986–9995.

23. Liu, Y.; Yang, K.; Cheng, L.; Zhu, J.; Ma, X.; Xu, H.; Li, Y.; Guo, L.; Gu, H.; Liu, Z. PEGylated 2O3 core-shell magnetic nanoparticles: Potential theranostic applications and in vivo toxicity studies. Nanomed. Nanotechnol. Biol. Med. 2013, 9, 1077–1088.

24. Yin, P.T.; Pongkulapa, T.; Cho, H.-Y.; Han, J.; Pasquale, N.J.; Rabie, H.; Kim, J.-H.; Choi, J.-W.; Lee, K.-B. Overcoming Chemoresistance in Cancer via Combined MicroRNA Therapeutics with Anticancer Drugs Using Multifunctional Magnetic Core–Shell Nanoparticles. ACS Appl. Mater. Interfaces 2018, 10, 26954–26963.

25. Sattarahmady, N.; Zare, T.; Mehdizadeh, A.; Azarpira, N.; Heidari, M.; Lotfi, M.; Heli, H. Dextrin-coated zinc substituted cobalt-ferrite nanoparticles as an MRI contrast agent: In vitro and in vivo imaging studies. Colloids Surf. B Biointerfaces 2015, 129, 15–20.

26. Cheng, L.; Yang, K.; Li, Y.; Zeng, X.; Shao, M.; Lee, S.-T.; Liu, Z. Multifunctional nanoparticles for upconversion luminescence/MR multimodal imaging and magnetically targeted photothermal therapy. Biomaterials 2012, 33, 2215–2222.

27. Hsu, J.C.; Naha, P.C.; Lau, K.C.; Chhour, P.; Hastings, R.; Moon, B.F.; Stein, J.M.; Witschey, W.R.T.; McDonald, E.S.; Maidment, A.D.A.; et al. An all-in-one nanoparticle (AION) contrast agent for breast cancer screening with DEM-CT-MRI-NIRF imaging. Nanoscale 2018, 10, 17236–17248.

28. Feng, L.; Wang, C.; Li, C.; Gai, S.; He, F.; Li, R.; An, G.; Zhong, C.; Dai, Y.; Yang, Z.; et al. Multifunctional Theranostic Nanoplatform Based on Fe-mTa2O5@CuS-ZnPc/PCM for Bimodal Imaging and Synergistically Enhanced Phototherapy. Inorg. Chem. 2018, 57, 4864–4876.

29. Song, G.; Chen, M.; Zhang, Y.; Cui, L.; Qu, H.; Zheng, X.; Wintermark, M.; Liu, Z.; Rao, J. Janus Iron Oxides @ Semiconducting Polymer Nanoparticle Tracer for Cell Tracking by Magnetic Particle Imaging. Nano Lett. 2018, 18, 182–189.

30. Tsoukalas, C.; Psimadas, D.; Kastis, G.A.; Koutoulidis, V.; Harris, A.L.; Paravatou-Petsotas, M.; Karageorgou, M.; Furenlid, L.R.; Moulopoulos, L.; Stamopoulos, D.; et al. A Novel Metal-Based Imaging Probe for Targeted Dual-Modality SPECT/MR Imaging of Angiogenesis. Front. Chem. 2018, 6, 224.

31. Roy, K.; Kanwar, R.K.; Kanwar, J.R. LNA aptamer based multi-modal, Fe3O4 -saturated lactoferrin (Fe3O4-bLf) nanocarriers for triple positive (EpCAM, CD133, CD44) colon tumor targeting and NIR, MRI and CT imaging. Biomaterials 201

5, 71, 84–99.

32. Xu, H.; Cheng, L.; Wang, C.; Ma, X.; Li, Y.; Liu, Z. Polymer encapsulated upconversion nanoparticle/iron oxide nanoco mposites for multimodal imaging and magnetic targeted drug delivery. Biomaterials 2011, 32, 9364–9373.

33. Yao, Y.; Zhao, D.; Li, N.; Shen, F.; Machuki, J.O.; Yang, D.; Li, J.; Tang, D.; Yu, Y.; Tian, J.; et al. Multifunctional Fe3O4 @ Molecular Machine for Magnetically Targeted Intracellular Zn2+ Imaging and Fluorescence/MRI Guided Photodynam ic-Photothermal Therapy. Anal. Chem. 2019, 91, 7850–7857.

34. Liu, T.; Shi, S.; Liang, C.; Shen, S.; Cheng, L.; Wang, C.; Song, X.; Goel, S.; Barnhart, T.; Cai, W.; et al. Iron Oxide Dec orated MoS2 Nanosheets with Double PEGylation for Chelator-Free Radiolabeling and Multimodal Imaging Guided Ph otothermal Therapy. ACS Nano 2015, 9, 950–960.

35. Wang, C.; Xu, H.; Liang, C.; Liu, Y.; Li, Z.; Yang, G.; Cheng, L.; Li, Y.; Liu, Z. Iron Oxide @ Polypyrrole Nanoparticles as a Multifunctional Drug Carrier for Remotely Controlled Cancer Therapy with Synergistic Antitumor Effect. ACS Nano 20 13, 7, 6782–6795.

36. Yuan, P.; Song, D. MRI tracing non-invasive TiO2-based nanoparticles activated by ultrasound for multi-mechanism the rapy of prostatic cancer. Nanotechnology 2018, 29, 125101.

37. Ye, D.-X.; Ma, Y.-Y.; Zhao, W.; Cao, H.-M.; Kong, J.-L.; Xiong, H.-M.; Möhwald, H. ZnO-Based Nanoplatforms for Labeli ng and Treatment of Mouse Tumors without Detectable Toxic Side Effects. ACS Nano 2016, 10, 4294–4300.

38. Li, Y.; Song, K.; Cao, Y.; Peng, C.; Yang, G. Keratin-Templated Synthesis of Metallic Oxide Nanoparticles as MRI Contr ast Agents and Drug Carriers. ACS Appl. Mater. Interfaces 2018, 10, 26039–26045.

39. Zhong, X.; Wang, X.; Zhan, G.; Tang, Y.; Yao, Y.; Dong, Z.; Hou, L.; Zhao, H.; Zeng, S.; Hu, J.; et al. NaCeF4:Gd,Tb Sci ntillator as an X-ray Responsive Photosensitizer for Multimodal Imaging-Guided Synchronous Radio/Radiodynamic Th erapy. Nano Lett. 2019, 19, 8234–8244.

40. Wang, Y.; Song, S.; Liu, J.; Liu, D.; Zhang, H. ZnO-Functionalized Upconverting Nanotheranostic Agent: Multi-Modality Imaging-Guided Chemotherapy with On-Demand Drug Release Triggered by pH. Angew. Chem. Int. Ed. 2014, 54, 536 –540.

41. Yang, G.; Xu, L.; Chao, Y.; Xu, J.; Sun, X.; Wu, Y.; Peng, R.; Liu, Z. Hollow MnO2 as a tumor-microenvironment-respon sive biodegradable nano-platform for combination therapy favoring antitumor immune responses. Nat. Commun. 2017, 8, 1–13.

42. Dong, Z.; Feng, L.; Chao, Y.; Chen, M.; Gao, M.; Zhao, H.; Zhu, W.; Liu, J.; Liang, C.; Zhang, Q.; et al. Synthesis of Holl ow Biomineralized CaCO3–Polydopamine Nanoparticles for Multimodal Imaging-Guided Cancer Photodynamic Therap y with Reduced Skin Photosensitivity. J. Am. Chem. Soc. 2018, 140, 2165–2178.

43. Dong, Z.; Gong, H.; Gao, M.; Liangzhu, F.; Sun, X.; Feng, L.; Fu, T.; Ziliang, D.; Liu, Z. Polydopamine Nanoparticles as a Versatile Molecular Loading Platform to Enable Imaging-guided Cancer Combination Therapy. Theranostics 2016, 6, 1031–1042.

44. Gao, Y.; Zhang, L.; Liu, Y.; Sun, S.; Yin, Z.; Zhang, L.; Li, A.; Lu, G.; Wu, A.; Zeng, L. Ce6/Mn 2+-chelated 2 nanoprobes for enhanced synergistic phototherapy and magnetic resonance imaging in 4T1 breast cancer. Nanoscale 2020, 12, 18 01–1810.

45. Zheng, T.; Wang, W.; Wu, F.; Zhang, M.; Shen, J.; Sun, Y. Zwitterionic Polymer-Gated 2 Core-Shell Nanoparticles for Im aging-Guided Combined Cancer Therapy. Theranostics 2019, 9, 5035–5048.

46. Yang, Y.; Liu, J.; Liang, C.; Feng, L.; Fu, T.; Dong, Z.; Chao, L.; Li, Y.; Lu, G.; Chen, M.; et al. Nanoscale Metal–Organic Particles with Rapid Clearance for Magnetic Resonance Imaging-Guided Photothermal Therapy. ACS Nano 2016, 10, 2 774–2781.

47. Liu, J.; Tian, L.; Zhang, R.; Dong, Z.; Wang, H.; Liu, Z. Collagenase-Encapsulated pH-Responsive Nanoscale Coordina tion Polymers for Tumor Microenvironment Modulation and Enhanced Photodynamic Nanomedicine. ACS Appl. Mater. I nterfaces 2018, 10, 43493–43502.

48. Dong, Z.; Feng, L.; Zhu, W.; Sun, X.; Gao, M.; Zhao, H.; Chao, Y.; Liu, Z. CaCO3 nanoparticles as an ultra-sensitive tu mor-pH-responsive nanoplatform enabling real-time drug release monitoring and cancer combination therapy. Biomater ials 2016, 110, 60–70.

49. Gong, F.; Cheng, L.; Yang, N.; Betzer, O.; Feng, L.; Zhou, Q.; Li, Y.; Chen, R.; Popovtzer, R.; Liu, Z. Ultrasmall Oxygen-Deficient Bimetallic Oxide MnWO X Nanoparticles for Depletion of Endogenous GSH and Enhanced Sonodynamic Can cer Therapy. Adv. Mater. 2019, 31, e1900730.

50. Li, M.; Zhao, Q.; Yi, X.; Zhong, X.; Song, G.; Chai, Z.; Liu, Z.; Yang, K. @ZnS Core/Shell/Shell Nanoparticles for Magne tic Resonance Imaging and Enhanced Cancer Radiation Therapy. ACS Appl. Mater. Interfaces 2016, 8, 9557–9564.

51. Zhou, J.; Luo, P.; Sun, C.; Meng, L.; Ye, W.; Chen, S.; Du, B. A "win–win" nanoplatform: TiO2:Yb,Ho,F for NIR light-induced synergistic therapy and imaging. Nanoscale 2017, 9, 4244–4254.

52. Chen, Y.; Cheng, L.; Dong, Z.; Chao, Y.; Lei, H.; Zhao, H.; Wang, J.; Liu, Z. Degradable Vanadium Disulfide Nanostructures with Unique Optical and Magnetic Functions for Cancer Theranostics. Angew. Chem. Int. Ed. 2017, 56, 12991–12996.

53. Wu, X.; Yang, H.; Yang, W.; Chen, X.; Gao, J.; Gong, X.; Wang, H.; Duan, Y.; Wei, D.; Chang, J. Nanoparticle-based diagnostic and therapeutic systems for brain tumors. J. Mater. Chem. B 2019, 7, 4734–4750.

54. Cheng, Y.; Morshed, R.A.; Auffinger, B.; Tobias, A.L.; Lesniak, M.S. Multifunctional nanoparticles for brain tumor imaging and therapy. Adv. Drug Deliv. Rev. 2014, 66, 42–57.

55. Tang, W.; Dong, Z.; Zhang, R.; Yi, X.; Yang, K.; Jin, M.; Yuan, C.; Xiao, Z.; Liu, Z.; Cheng, L. Multifunctional Two-Dimensional Core–Shell Nanocomposites for Enhanced Photo–Radio Combined Therapy in the Second Biological Window. ACS Nano 2019, 13, 284–294.

56. Gao, K.; Tu, W.; Yu, X.; Ahmad, F.; Zhang, X.; Wu, W.; An, X.; Chen, X.; Li, W. W-doped TiO2 nanoparticles with strong absorption in the NIR-II window for photoacoustic/CT dual-modal imaging and synergistic thermoradiotherapy of tumors. Theranostics 2019, 9, 5214–5226.

57. Wang, X.; Wang, J.; Pan, J.; Zhao, F.; Kan, D.; Cheng, R.; Zhang, X.; Sun, S.-K. Rhenium Sulfide Nanoparticles as a Biosafe Spectral CT Contrast Agent for Gastrointestinal Tract Imaging and Tumor Theranostics in Vivo. ACS Appl. Mater. Interfaces 2019, 11, 33650–33658.

58. Zhen, W.; An, S.; Wang, W.; Liu, Y.; Jia, X.; Wang, C.; Zhang, M.; Jiang, X. Gram-scale fabrication of nanoparticles through one-step hydrothermal method for dual-model imaging-guided NIR-II photothermal therapy. Nanoscale 2019, 11, 9906–9911.

59. Liu, J.; Yang, G.; Zhu, W.; Dong, Z.; Yang, Y.; Chao, Y.; Liu, Z. Light-controlled drug release from singlet-oxygen sensitive nanoscale coordination polymers enabling cancer combination therapy. Biomaterials 2017, 146, 40–48.

60. Boll, H.; Nittka, S.; Doyon, F.; Neumaier, M.; Marx, A.; Kramer, M.; Groden, C.; Brockmann, M.A. Micro-CT Based Experimental Liver Imaging Using a Nanoparticulate Contrast Agent: A Longitudinal Study in Mice. PLoS ONE 2011, 6, e25692.

61. Kosaka, N.; Ogawa, M.; Choyke, P.L.; Kobayashi, H. Clinical implications of near-infrared fluorescence imaging in cancer. Future Oncol. 2009, 5, 1501–1511.

62. Puvvada, N.; Rajput, S.; Kumar, B.P.; Sarkar, S.; Konar, S.; Brunt, K.; Rao, R.R.; Mazumdar, A.; Das, S.K.; Basu, R.; et al. Novel ZnO hollow-nanocarriers containing paclitaxel targeting folate-receptors in a malignant pH-microenvironment for effective monitoring and promoting breast tumor regression. Sci. Rep. 2015, 5, 11760.

63. Chen, J.; Li, X.; Sun, Y.; Hu, Y.; Peng, Y.; Li, Y.; Yin, G.; Liu, H.; Xu, J.; Zhong, S. Synthesis of Size-Tunable Hollow Polypyrrole Nanostructures and Their Assembly into Folate-Targeting and pH-Responsive Anticancer Drug-Delivery Agents. Chem. Eur. J. 2017, 23, 17279–17289.

64. Xie, L.; Wang, G.; Zhou, H.; Zhang, F.; Guo, Z.; Liu, C.; Zhang, X.; Zhu, L. Functional long circulating single walled carbon nanotubes for fluorescent/photoacoustic imaging-guided enhanced phototherapy. Biomaterials 2016, 103, 219–228.

65. Yan, L.; Shi, H.; He, X.; Wang, K.; Tang, J.; Chen, M.; Ye, X.; Xu, F.; Lei, Y. A Versatile Activatable Fluorescence Probing Platform for Cancer Cells in Vitro and in Vivo Based on Self-Assembled Aptamer/Carbon Nanotube Ensembles. Anal. Chem. 2014, 86, 9271–9277.

66. Yu, J.; Diao, X.; Zhang, X.; Chen, X.; Hao, X.; Li, W.; Zhang, X.; Lee, C.-S. Water-Dispersible, pH-Stable and Highly-Luminescent Organic Dye Nanoparticles with Amplified Emissions for In Vitro and In Vivo Bioimaging. Small 2013, 10, 1125–1132.

67. Lu, G.-H.; Shang, W.-T.; Deng, H.; Han, Z.-Y.; Hu, M.; Liang, X.-Y.; Fang, C.-H.; Zhu, X.-H.; Fan, Y.-F.; Tian, J. Targeting carbon nanotubes based on IGF-1R for photothermal therapy of orthotopic pancreatic cancer guided by optical imaging. Biomaterials 2019, 195, 13–22.

68. Antaris, A.L.; Robinson, J.T.; Yaghi, O.K.; Hong, G.; Diao, S.; Luong, R.; Dai, H. Ultra-Low Doses of Chirality Sorted (6, 5) Carbon Nanotubes for Simultaneous Tumor Imaging and Photothermal Therapy. ACS Nano 2013, 7, 3644–3652.

69. Diao, S.; Hong, G.; Robinson, J.T.; Jiao, L.; Antaris, A.L.; Wu, J.Z.; Choi, C.L.; Dai, H. Chirality Enriched (12,1) and (11, 3) Single-Walled Carbon Nanotubes for Biological Imaging. J. Am. Chem. Soc. 2012, 134, 16971–16974.

70. Yi, H.; Ghosh, D.; Ham, M.-H.; Qi, J.; Barone, P.W.; Strano, M.S.; Belcher, A.M. M13 Phage-Functionalized Single-Walled Carbon Nanotubes As Nanoprobes for Second Near-Infrared Window Fluorescence Imaging of Targeted Tumors. Nano Lett. 2012, 12, 1176–1183.

71. Ghosh, D.; Bagley, A.F.; Na, Y.J.; Birrer, M.J.; Bhatia, S.N.; Belcher, A.M. Deep, noninvasive imaging and surgical guidance of submillimeter tumors using targeted M13-stabilized single-walled carbon nanotubes. Proc. Natl. Acad. Sci. USA 2014, 111, 13948–13953.

72. Wan, H.; Yue, J.; Zhu, S.; Uno, T.; Zhang, X.; Yang, Q.; Yu, K.; Hong, G.; Wang, J.; Li, L.; et al. A bright organic NIR-II nanofluorophore for three-dimensional imaging into biological tissues. Nat. Commun. 2018, 9, 1171.

73. Robinson, J.T.; Hong, G.; Liang, Y.; Zhang, B.; Yaghi, O.K.; Dai, H. In Vivo Fluorescence Imaging in the Second Near-Infrared Window with Long Circulating Carbon Nanotubes Capable of Ultrahigh Tumor Uptake. J. Am. Chem. Soc. 2012, 134, 10664–10669.

74. Miao, W.; Shim, G.; Lee, S.; Oh, Y.-K. Structure-dependent photothermal anticancer effects of carbon-based photoresponsive nanomaterials. Biomaterials 2014, 35, 4058–4065.

75. Diao, S.; Blackburn, J.L.; Hong, G.; Antaris, A.L.; Chang, J.; Wu, J.Z.; Zhang, B.; Cheng, K.; Kuo, C.J.; Dai, H. Fluorescence Imaging In Vivo at Wavelengths beyond 1500 nm. Angew. Chem. Int. Ed. 2015, 54, 14758–14762.

76. Ceppi, L.; Bardhan, N.M.; Na, Y.; Siegel, A.; Rajan, N.; Fruscio, R.; Del Carmen, M.G.; Belcher, A.M.; Birrer, M.J. Real-Time Single-Walled Carbon Nanotube-Based Fluorescence Imaging Improves Survival after Debulking Surgery in an Ovarian Cancer Model. ACS Nano 2019, 13, 5356–5365.

77. Liang, X.; Shang, W.; Chi, C.; Zeng, C.; Wang, K.; Fang, C.; Chen, Q.; Liu, H.; Fan, Y.; Tian, J. Dye-conjugated single-walled carbon nanotubes induce photothermal therapy under the guidance of near-infrared imaging. Cancer Lett. 2016, 383, 243–249.

78. Zhang, F.; Cao, J.; Chen, X.; Yang, K.; Zhu, L.; Fu, G.; Huang, X.; Chen, X. Noninvasive Dynamic Imaging of Tumor Early Response to Nanoparticle-mediated Photothermal Therapy. Theranostics 2015, 5, 1444–1455.

79. Chen, Q.; Wang, C.; Zhan, Z.; He, W.; Cheng, Z.; Li, Y.; Liu, Z. Near-infrared dye bound albumin with separated imaging and therapy wavelength channels for imaging-guided photothermal therapy. Biomaterials 2014, 35, 8206–8214.

80. Yu, N.; Hu, Y.; Wang, X.; Liu, G.; Wang, Z.; Liu, Z.; Tian, Q.; Zhu, M.; Shi, X.; Chen, Z. Dynamically tuning near-infrared-induced photothermal performances of TiO2 nanocrystals by Nb doping for imaging-guided photothermal therapy of tumors. Nanoscale 2017, 9, 9148–9159.

81. Yang, Y.; An, F.; Liu, Z.; Zhang, X.; Zhou, M.; Li, W.; Hao, X.; Lee, C.-S.; Zhang, X. Ultrabright and ultrastable near-infrared dye nanoparticles for in vitro and in vivo bioimaging. Biomaterials 2012, 33, 7803–7809.

82. Dang, X.; Gu, L.; Qi, J.; Correa, S.; Zhang, G.; Belcher, A.M.; Hammond, P.T. Layer-by-layer assembled fluorescent probes in the second near-infrared window for systemic delivery and detection of ovarian cancer. Proc. Natl. Acad. Sci. USA 2016, 113, 5179–5184.

83. He, Y.; Zhong, Y.; Su, Y.; Lu, Y.; Jiang, Z.; Peng, F.; Xu, T.; Su, S.; Huang, Q.; Fan, C.; et al. Water-Dispersed Near-Infrared-Emitting Quantum Dots of Ultrasmall Sizes for In Vitro and In Vivo Imaging. Angew. Chem. Int. Ed. 2011, 50, 5695–5698.

84. Lu, Y.; Zhong, Y.; Wang, J.; Su, Y.; Peng, F.; Zhou, Y.; Jiang, X.; He, Y. Aqueous synthesized near-infrared-emitting quantum dots for RGD-basedin vivoactive tumour targeting. Nanotechnology 2013, 24, 135101.

85. Welsher, K.; Liu, Z.; Sherlock, S.P.; Robinson, J.T.; Chen, Z.; Daranciang, D.; Dai, H. A route to brightly fluorescent carbon nanotubes for near-infrared imaging in mice. Nat. Nanotechnol. 2009, 4, 773–780.

86. Xiang, L.; Yuan, Y.; Xing, D.; Ou, Z.; Yang, S.; Zhou, F. Photoacoustic molecular imaging with antibody-functionalized single-walled carbon nanotubes for early diagnosis of tumor. J. Biomed. Opt. 2009, 14, 021008.

87. De La Zerda, A.; Bodapati, S.; Teed, R.; May, S.Y.; Tabakman, S.M.; Liu, Z.; Khuri-Yakub, B.T.; Chen, X.; Dai, H.; Gambhir, S.S. Family of Enhanced Photoacoustic Imaging Agents for High-Sensitivity and Multiplexing Studies in Living Mice. ACS Nano 2012, 6, 4694–4701.

88. Zanganeh, S.; Li, H.; Kumavor, P.D.; Alqasemi, U.S.; Aguirre, A.; Mohammad, I.; Stanford, C.; Smith, M.B.; Zhu, Q. Photoacoustic imaging enhanced by indocyanine green-conjugated single-wall carbon nanotubes. J. Biomed. Opt. 2013, 18, 096006.

89. Shi, S.; Xu, C.; Yang, K.; Goel, S.; Valdovinos, H.; Luo, H.; Ehlerding, E.B.; England, C.G.; Cheng, L.; Chen, F.; et al. Chelator-Free Radiolabeling of Nanographene: Breaking the Stereotype of Chelation. Angew. Chem. Int. Ed. 2017, 56, 2889–2892.

90. Qiu, Y.; Ding, D.; Sun, W.; Feng, Y.; Huang, D.; Li, S.; Meng, S.; Zhao, Q.; Xue, L.-J.; Chen, H. Hollow mesoporous carbon nanospheres for imaging-guided light-activated synergistic thermo-chemotherapy. Nanoscale 2019, 11, 16351–16361.

91. Zhou, L.; Jing, Y.; Liu, Y.; Liu, Z.; Gao, D.; Chen, H.; Song, W.; Wang, T.; Fang, X.; Qin, W.; et al. Mesoporous Carbon Nanospheres as a Multifunctional Carrier for Cancer Theranostics. Theranostics 2018, 8, 663–675.

92. Jiao, X.; Zhang, W.; Zhang, L.; Cao, Y.; Xu, Z.; Kang, Y.; Xue, P. Rational design of oxygen deficient TiO2−x nanoparticles conjugated with chlorin e6 (Ce6) for photoacoustic imaging-guided photothermal/photodynamic dual therapy of cancer. Nanoscale 2020, 12, 1707–1718.

93. Zhong, J.; Wen, L.; Yang, S.; Xiang, L.; Chen, Q.; Xing, D. Imaging-guided high-efficient photoacoustic tumor therapy with targeting gold nanorods. Nanomed. Nanotechnol. Biol. Med. 2015, 11, 1499–1509.

94. Zhang, L.; Chen, Q.; Zou, X.; Chen, J.; Hu, L.; Dong, Z.; Zhou, J.; Chen, Y.; Liu, Z.; Cheng, L. Intelligent protein-coated bismuth sulfide and manganese oxide nanocomposites obtained by biomineralization for multimodal imaging-guided enhanced tumor therapy. J. Mater. Chem. B 2019, 7, 5170–5181.

95. Zhang, R.; Fan, X.; Meng, Z.; Lin, H.; Jin, Q.; Gong, F.; Dong, Z.; Li, Y.; Chen, Q.; Liu, Z.; et al. Renal Clearable Ru-based Coordination Polymer Nanodots for Photoacoustic Imaging Guided Cancer Therapy. Theranostics 2019, 9, 8266–8276.

96. Liu, Z.; Tabakman, S.M.; Chen, Z.; Dai, H. Preparation of carbon nanotube bioconjugates for biomedical applications. Nat. Protoc. 2009, 4, 1372–1381.

97. De La Zerda, A.; Zavaleta, C.; Keren, S.; Vaithilingam, S.; Bodapati, S.; Liu, Z.; Levi, J.; Smith, B.R.; Ma, T.-J.; Oralkan, O.; et al. Carbon nanotubes as photoacoustic molecular imaging agents in living mice. Nat. Nanotechnol. 2008, 3, 557–562.

98. McDevitt, M.; Ruggiero, A.; Villa, C.H.; Holland, J.; Sprinkle, S.R.; May, C.; Lewis, J.; Scheinberg, D. Imaging and treating tumor vasculature with targeted radiolabeled carbon nanotubes. Int. J. Nanomed. 2010, 5, 783–802.

99. Shi, S.; Yang, K.; Hong, H.; Chen, F.; Valdovinos, H.; Goel, S.; Barnhart, T.; Liu, Z.; Cai, W. VEGFR targeting leads to significantly enhanced tumor uptake of nanographene oxide in vivo. Biomaterials 2015, 39, 39–46.

100. Hong, H.; Wang, F.; Zhang, Y.; Graves, S.A.; Eddine, S.B.Z.; Yang, Y.; Theuer, C.P.; Nickles, R.J.; Wang, X.; Cai, W. Red Fluorescent Zinc Oxide Nanoparticle: A Novel Platform for Cancer Targeting. ACS Appl. Mater. Interfaces 2015, 7, 3373–3381.

101. Li, L.; Li, J.; Shi, Y.; Du, P.; Zhang, Z.; Liu, T.; Zhang, R.; Liu, Z. On-Demand Biodegradable Boron Nitride Nanoparticles for Treating Triple Negative Breast Cancer with Boron Neutron Capture Therapy. ACS Nano 2019, 13, 13843–13852.

102. Dong, Z.; Feng, L.; Chao, Y.; Chen, M.; Gong, F.; Han, X.; Zhang, R.; Cheng, L.; Liu, Z. Amplification of Tumor Oxidative Stresses with Liposomal Fenton Catalyst and Glutathione Inhibitor for Enhanced Cancer Chemotherapy and Radiotherapy. Nano Lett. 2019, 19, 805–815.

103. Gaté, L.; Disdier, C.; Cosnier, F.; Gagnaire, F.; Devoy, J.; Saba, W.; Brun, E.; Chalansonnet, M.; Mabondzo, A. Biopersistence and translocation to extrapulmonary organs of titanium dioxide nanoparticles after subacute inhalation exposure to aerosol in adult and elderly rats. Toxicol. Lett. 2017, 265, 61–69.

104. Wu, H.; Shi, H.; Zhang, H.; Wang, X.; Yang, Y.; Yu, C.; Hao, C.; Du, J.; Hu, H.; Yang, S. Prostate stem cell antigen antibody-conjugated multiwalled carbon nanotubes for targeted ultrasound imaging and drug delivery. Biomaterials 2014, 35, 5369–5380.

105. Mehrmohammadi, M.; Shin, T.-H.; Qu, M.; Kruizinga, P.; Truby, R.L.; Lee, J.-H.; Cheon, J.; Emelianov, S.Y. In vivo pulsed magneto-motive ultrasound imaging using high-performance magnetoactive contrast nanoagents. Nanoscale 2013, 5, 11179–11186.

106. Chen, L.; Zhong, X.; Yi, X.; Huang, M.; Ning, P.; Liu, T.; Ge, C.; Chai, Z.; Liu, Z.; Yang, K. Radionuclide 131I labeled reduced graphene oxide for nuclear imaging guided combined radio- and photothermal therapy of cancer. Biomaterials 2015, 66, 21–28.